Multiple-Band Linear-Polarization Conversion and Circular Polarization in Reflection Mode Using a Symmetric Anisotropic Metasurface

Bao-Qin Lin,* Jian-Xin Guo, Peng Chu, Wen-Jun Huo, Zhuo Xing, Bai-Gang Huang, and Lan Wu
School of Information Engineering, Xijing University, Xi'an 710123, China

(Received 25 May 2017; revised manuscript received 15 November 2017; published 28 February 2018)

In this work, we propose a multiband linear-polarization (LP) conversion and circular polarization (CP) maintaining reflector using a symmetric anisotropic metasurface. The anisotropic metasurface is composed of a square array of a two-corner-cut square multiring disk printed on a grounded dielectric substrate, which is a symmetric structure with a pair of mutually perpendicular symmetric axes u and v along the $\pm 45°$ directions with respect to the y-axis direction. The simulated results show that the reflector can realize LP conversion in five frequency bands at both x- and y-polarized incidence, the first four bands all have a certain bandwidth, and the fourth one, especially, is an ultrawideband. In addition, because of the symmetry of the reflector structure, the polarization state of a CP wave can be maintained after reflection, and the magnitude of the copolarized reflection coefficient at the CP incidence is just equal to that of the cross-polarized reflection coefficient at the x- and y-polarized incidence. We analyze the root cause of the multiband LP conversion and CP maintaining reflection, and carry out one experiment to verify the proposed reflector.

DOI: 10.1103/PhysRevApplied.9.024038

I. INTRODUCTION

Polarization is an expression of the orientation of the electric flux lines in an electromagnetic (EM) wave, which is an important characteristic of the EM wave. It is essential to manipulating the polarization state of an EM wave for various EM applications, such as radio communication, antenna design, radar technology, and radar stealth technology [1–4]. Conventional methods of controlling polarization are usually realized by using the birefringence effect and optical activity of natural materials, which usually suffers from bulky volumes, high losses, and a narrow bandwidth in practical applications [5–6]. Over the past decade, it has been found that metamaterials (MMs) can provide a convenient way to control the polarization state of an EM wave. Based on various MMs, many different polarization converters have been proposed [7–39]. They are usually realized in one of the following two methods: one is to divide an EM wave into two orthogonal components and generate a different phase between them (the fundamental of birefringence effect) by using anisotropic MMs. The other one is to mimic molecule chirality (the fundamental of optical activity) by using chiral MMs. The existing literature indicates that the two methods can both be used to design various polarization converters, we can choose a proper design method according to the different work patterns of various polarization converters. Anisotropic two-dimensional MM (also called metasurface) is suitable for the design of reflective polarization converters, especially using multiple plasmon resonances, high-efficiency and ultrawideband polarization converters can be achieved in this way [7–14]. For example, Ref. [8] presents a reflective polarization converter based on a double V-shaped anisotropic metasurface, which can realize an ultrawideband LP conversion due to four plasmon resonances. In Ref. [13], another ultrawideband polarization converter is proposed, which is composed of three resonators. However, chiral MM is convenient for designing transmissive polarization converters. Most presented transmissive circular or linear-polarization converters are realized by using planar [15–22] or 3D [23–26] chiral MMs. Moreover, in many cases, an asymmetric transmission effect can be achieved at the same time due to the asymmetry of the chiral MM structures [27–30]. In recent years, to improve the practical applicability of polarization converters ulteriorly, many researchers have been focused on achieving high-efficiency multiband polarization conversion. Recently, a number of multiband reflective [31–35] and transmissive [36–38] polarization converters have been proposed based on various MMs, which can realize effective linear- or circular-polarization conversion in three-to-five frequency bands. However, their frequency bands are usually not wide. Though the two polarization converters in Refs. [33,36] both have a wideband with about 25% relative bandwidth, they have only three frequency bands in all in each one. It is shown that the practical applicability of these presented multiband polarization converters is still not strong, and it is necessary to continue in-depth research in this respect. In addition, a

*aflbq@sina.com

right-handed or left-handed circular-polarized (RHCP or LHCP) wave will be converted to a LHCP (RHCP) wave after reflection on a conducting surface. While the polarization state of a circular-polarized (CP) wave can be maintained after reflection on a CP-maintaining metasurface, it is similar to a CP conversion in transmission mode. This kind of CP-maintaining metasurface has been regarded as a kind of reflective CP converter in Ref. [39]. When the CP-maintaining metasurface is designed as a CP phase gradient metasurface through the rotating of subunit cells, or it is coplanar with the conductor surface alternately, the direction of the reflected wave at the CP incidence will be changed, and the RCS of the stealth target in some directions can be reduced. In recent years, this kind of CP-maintaining metasurface has drawn much attention, and a few effective designs have been proposed [39–43].

In this work, we propose a reflector based on an anisotropic metasurface, which is a symmetric structure with a pair of mutually perpendicular symmetric axes u and v along ±45° directions with respect to the y axis. It can realize multiband LP conversion for its unit cell is composed of four resonators. The simulated results show that LP conversion can be achieved in five frequency bands at x- and y-polarized incidence. The first four bands all have a certain bandwidth, especially the fourth one is an ultrawideband with 36.8% relative bandwidth. In addition, one derived formula shows that the magnitude of the copolarized reflection coefficient at RHCP and LHCP incidence is just equal to that of the cross-polarized reflection coefficient at x- and y-polarized incidence, the reflector can realize a multiband CP-maintaining reflection at the same time. We analyze the root cause of the multiband LP conversion and CP-maintaining reflection, and conclude that because different eigenmodes are excited in the anisotropic unit cell structure at v- and u-polarized incidences, a phase difference between the two reflected coefficients r_{uu} and r_{vv} will be generated. The phase difference can basically determine the magnitudes of the cross- and copolarized reflected coefficients at y-polarized incidence. When the phase difference is close to 180°, the anticipated polarization conversion can be realized. In addition, the reflected coefficients at y- and x-polarized incidences are completely equal at all times for the symmetry of the reflector structure, and such a multiband CP-maintaining reflection can be realized at the same time.

II. DESIGN AND SIMULATION

The unit cell of the proposed reflector is composed of a two-corner-cut square disk surrounded by three concentric isomorphous rings, which are all printed on a grounded dielectric substrate, as shown in Fig. 1. The geometrical parameters of the unit cell are chosen as follows: $P = 12.00$ mm, $a = 1.98$ mm, $b = 4.52$ mm, $d = 0.30$ mm, $w = 0.45$ mm, and $h = 3.60$ mm (see Fig. 1). In addition, the metallic layer, together with the grounded plane, is

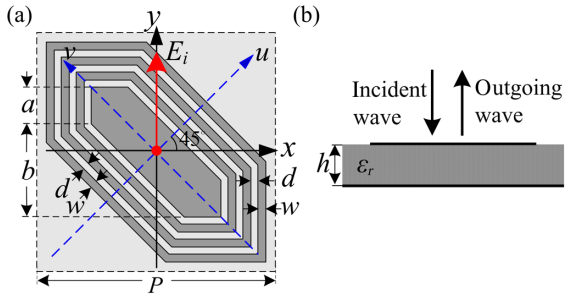

FIG. 1. Unit cell of the proposed reflector. (a) Top view, (b) side view.

modeled as a 0.017-mm copper film with an electric conductivity of $\sigma = 5.8 \times 10^7$ S/m, and the dielectric substrate is selected as a RT/duroid 4730 with a relative permittivity of 3.0 and a dielectric loss tangent of 0.0013.

Owing to the anisotropy of the reflector structure, when a common LP plane wave is incident on it, the reflected electric fields would consist of both cross- and copolarized components, we utilize a reflection matrix $\mathbf{R}_{\text{lin}}$ to describe the relationships between incident and reflected electric fields as

$$\begin{pmatrix} E_x^r \\ E_y^r \end{pmatrix} = \begin{pmatrix} r_{xx} & r_{xy} \\ r_{yx} & r_{yy} \end{pmatrix} \begin{pmatrix} E_x^i \\ E_y^i \end{pmatrix} = R_{\text{lin}} \begin{pmatrix} E_x^i \\ E_y^i \end{pmatrix}, \quad (1)$$

wherein $r_{ij} = E_i^r / E_j^i$, the first and the second subscripts i and j correspond to the polarized states of the reflected and incident fields, respectively, and another subscript *lin* indicates the LP wave. Based on formula (1), we can further derive another reflection matrix $\mathbf{R}_{\text{cir}}$ for the CP wave as follows:

$$\begin{aligned} \begin{pmatrix} E_+^r \\ E_-^r \end{pmatrix} &= \begin{pmatrix} r_{++} & r_{+-} \\ r_{-+} & r_{--} \end{pmatrix} \begin{pmatrix} E_+^i \\ E_-^i \end{pmatrix} = R_{\text{cir}} \begin{pmatrix} E_+^i \\ E_-^i \end{pmatrix} \\ &= \frac{1}{2} \begin{pmatrix} r_{xx} - r_{yy} - j(r_{xy} + r_{yx}) & r_{xx} + r_{yy} + j(r_{xy} - r_{yx}) \\ r_{xx} + r_{yy} - j(r_{xy} - r_{yx}) & r_{xx} - r_{yy} + j(r_{xy} + r_{yx}) \end{pmatrix} \\ &\quad \times \begin{pmatrix} E_+^i \\ E_-^i \end{pmatrix}, \end{aligned} \quad (2)$$

wherein the subscripts + and − denote RHCP and LHCP states, respectively. The polarization conversion ratio (PCR) for the y- or x-polarized incident wave can be calculated as

$$\begin{aligned} &\text{PCR} = |r_{xy}|^2 / (|r_{xy}|^2 + |r_{yy}|^2) \\ \text{or} \quad &\text{PCR} = |r_{yx}|^2 / (|r_{yx}|^2 + |r_{xx}|^2). \end{aligned} \quad (3)$$

In addition, we define a polarization-maintaining ratio (PMR) for the RHCP (LHCP) wave as

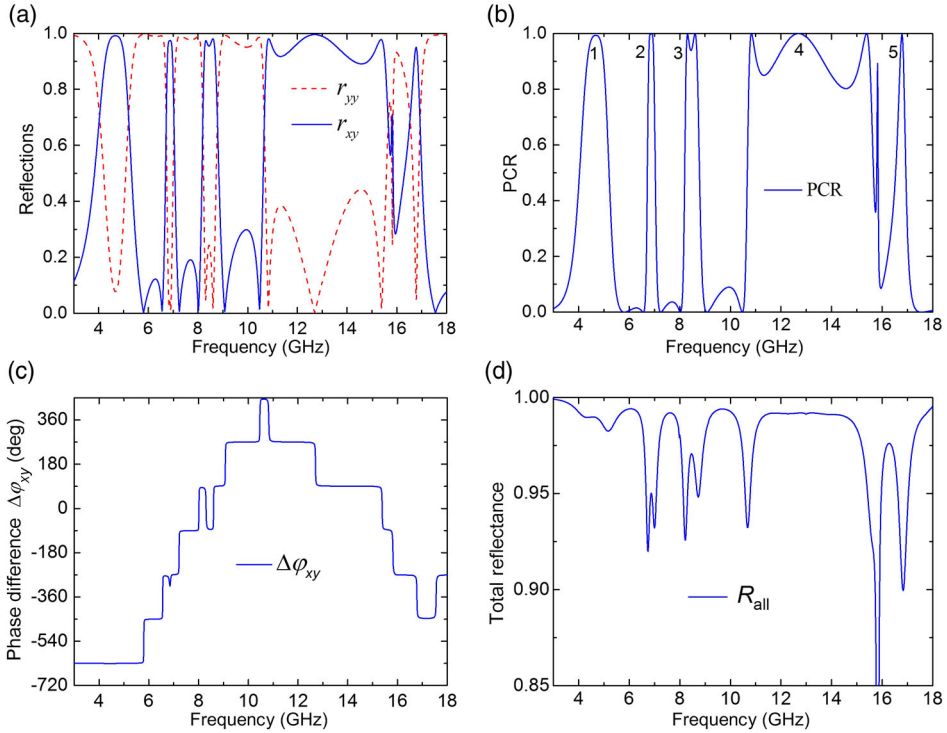

FIG. 2. Simulated results of the reflector at y-polarized incidence: (a) the magnitudes of r_{xy} and r_{yy}, (b) the polarization-conversion ratio (PCR), (c) the phase difference $\Delta\varphi_{xy}$ between r_{xy} and r_{yy}, and (d) the total reflectance R_{all}.

$$\text{PMR} = |r_{++}|^2/(|r_{++}|^2 + |r_{-+}|^2)$$
$$\text{or} \quad \text{PMR} = |r_{--}|^2/(|r_{+-}|^2 + |r_{--}|^2). \tag{4}$$

To numerically investigate the performance of our design, we suppose that the reflector is located in the X-Y plane and several plane EM waves with different polarizations are incident on the reflector in the sequence. First, the incident wave is assumed as a y-polarized one $E^i = E_0 e^{-jkz}\hat{e}_y$, as the simulated results using the commercial software CST Microwave Studio, the magnitudes of r_{xy} and r_{yy}, together with the PCR, the phase difference $\Delta\varphi_{xy} = \arg(r_{xy}) - \arg(r_{yy})$ and the total reflectance $R_{\text{all}} = |r_{xy}|^2 + |r_{yy}|^2$, are all shown in Fig. 2, it is indicated that the anticipated polarization conversion is realized in five bands. The former three bands are found in the frequency ranges 4.34–4.98 GHz, 6.77–6.97 GHz, and 8.25–8.69 GHz, respectively, wherein the PCR are over 90%, and the bandwidths of the three bands are 0.64, 0.20, and 0.44 GHz, respectively. In the fourth band, the minimum of the PCR is still 80.5%, if we regard PCR $\geq$ 80% as the criterion for the judgment of polarization conversion now, it is an ultrawideband (10.72–15.56 GHz) with 36.8% relative bandwidth. However, the fifth band is a narrow one (16.71–16.84 GHz), wherein only one maximum value exsits. In Fig. 2(a), it is indicated that the magnitude of r_{xy} is just equal to that of r_{yy} at the twelve frequencies: 4.04, 5.20, 6.72, 7.03, 8.19, 8.78, 10.67, 15.66, 15.78, 15.84, 16.53, and 16.94, $|r_{xy}| = |r_{yy}| \approx 0.7$. At the same time, Fig. 2(c) indicates the phase difference $\Delta\varphi_{xy} = \arg(r_{xy}) - \arg(r_{yy})$ is close to $\pm(2n+1)90°$ at all of these frequencies. It is implied that the y-polarized incident wave has been converted to a CP-reflected wave at the twelve frequencies. Furthermore, in Fig. 2(d), it is shown that the total reflectance R_{all} is a minimal value at the ten frequencies: 4.35, 5.17, 6.74, 7.00, 8.20, 8.73, 10.68, 15.58, 15.82, and 16.83. In fact, the reflector has a grounded plane; no transmission exists. In addition, in the simulation, the reflector is regarded as an infinite two-dimensional planar periodic structure. The simulation model is only one unit cell, which is separated from the adjacent unit cells using periodic boundaries. When an incident wave is introduced through the Floquet port, the electromagnetic energy cannot be transmitted to the adjacent unit cells laterally. The total reflectance R_{all} is less than 1.0 now. It is implied that there is dielectric loss in the dielectric substrate and a little electromagnetic energy has been transferred into heat energy. Because the dielectric loss tangent of the dielectric substrate is a constant (0.0013), the dielectric loss will be proportional to the square of the electric field in the dielectric substrate. At the above-mentioned ten-frequency points, the total reflectance R_{all} has been a regional minimum value. It is implied that the magnitudes of the dielectric loss and the electric field in the dielectric substrate have been a regional maximum value, and spoof surface plasmon resonances have been excited at these frequencies. Finally, from the comparison between Figs. 2(b) and 2(d), it is indicated that the ten resonant frequencies are all close to the transformation points of the PCR, what is the root cause of it? We will analyze it in detail in the next section.

The above results are obtained at y-polarized incidence, as the simulated results, we have obtained the reflected

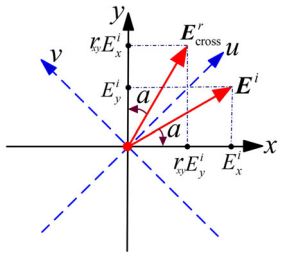

FIG. 3. Intuitive picture of the CP-maintaining reflection in the proposed reflector.

coefficients at x-polarized incidence at the same time, it is shown that $r_{yy} = r_{xx}$ and $r_{xy} = r_{yx}$. This is because the reflector is a symmetric structure with a pair of mutually perpendicular symmetric axes u and v along $\pm 45°$ directions with respect to the y axis, as shown in Fig. 1. Especially the symmetric axis u is just the angle bisector of the right angle between the x and y axis. This indicates that the x and y axes are symmetrical in the reflector structure, so the reflected coefficients at y- and x-polarized incidences are completely equal at all times.

In succession, we assume that one RHCP or LHCP wave is incident normally on the reflector. According to the reflected coefficients at y- and x-polarized incidences, the reflected coefficients at RHCP or LHCP incidences can be obtained by using formula (2). Because of $r_{yy} = r_{xx}$ and $r_{xy} = r_{yx}$ now, according to formula (2), the reflection matrix $\mathbf{R}_{\text{cir}}$ can be simplified as

$$R_{\text{cir}} = \begin{pmatrix} r_{++} & r_{+-} \\ r_{-+} & r_{--} \end{pmatrix} = \begin{pmatrix} -ir_{xy} & r_{yy} \\ r_{yy} & ir_{xy} \end{pmatrix}. \tag{5}$$

It is shown the magnitudes of the copolarized reflections at RHCP and LHCP incidences are just equal to those of the cross-polarized reflections at x- or y-polarized incidence $|r_{++}| = |r_{--}| = |r_{xy}| = |r_{yx}|$, and r_{-+} and r_{+-} are completely equal to r_{yy} and r_{xx}. Moreover, PMR $= |r_{++}|^2/(|r_{++}|^2 + |r_{-+}|^2) = |r_{xy}|^2/(|r_{xy}|^2 + |r_{yy}|^2)$=PCR. Why does the reflector have this anomalous multiband CP-maintaining reflection performance? We show one intuitive picture in Fig. 3, which indicates the magnitude and direction of the incident and reflected electric field vector in a fixed plane that is close and parallel to the reflector surface. The incident electric field is assumed as $E^i = E^i_x\hat{e}_x + E^i_y\hat{e}_y$, due to the polarization conversions at x- and y-polarized incidences, the cross-polarized reflected field will be generated, which can be expressed as $E^r_{\text{cross}} = r_{xy}E^i_y\hat{e}_x + r_{yx}E^i_x\hat{e}_y = r_{xy}(E^i_y\hat{e}_x + E^i_x\hat{e}_y)$ due to $r_{xy} = r_{yx}$, such that the symmetric axes u will always be the angle bisector of the intersection angle between E^i and E^r_{cross}, and the magnitude ratio between E^i and E^r_{cross} is just $|r_{xy}|$. When E^i is in a CP incidence and rotated clockwise or anticlockwise, the rotation direction of E^r_{cross} will be reversed, such that the polarization state of the reflected wave will keep the same as that of the incident wave because the propagating direction of the reflected wave will also be reversed. In this way, a CP-maintaining reflection can be achieved; moreover, $|r_{++}| = |r_{--}| = |r_{xy}| = |r_{yx}|$.

III. THEORETICAL ANALYSIS

To get a physical insight into the root cause of the multiband polarization conversion for the proposed reflector, we present a detailed analysis in succession.

First, we assume that the incidence is a u- or v-polarized wave, in which the incident fields E^i can be decomposed into x and y components, and the magnitudes of the two components are exactly equal. The incident field can be expressed as $E^i = E^i_u\hat{e}_u = E^i_y\hat{e}_y + E^i_x\hat{e}_x = E^i\cos(45°)(\hat{e}_y + \hat{e}_x)$ or $E^i = E^i_v\hat{e}_v = E^i_y\hat{e}_y + E^i_x\hat{e}_x = E^i\cos(45°)(\hat{e}_y - \hat{e}_x)$. Because of $r_{yy} = r_{xx}$ and $r_{xy} = r_{yx}$, the reflected field E^r is calculated as follows:

$$\begin{aligned} E^r|_u &= \begin{pmatrix} E^r_x \\ E^r_y \end{pmatrix}\Big|_u = \begin{pmatrix} r_{xx} & r_{xy} \\ r_{yx} & r_{yy} \end{pmatrix}\begin{pmatrix} E^i\cos(45°) \\ E^i\cos(45°) \end{pmatrix} \\ &= \begin{pmatrix} r_{yy} & r_{xy} \\ r_{xy} & r_{yy} \end{pmatrix}\begin{pmatrix} E^i\cos(45°) \\ E^i\cos(45°) \end{pmatrix}, \quad \text{or} \\ E^r|_v &= \begin{pmatrix} E^r_x \\ E^r_y \end{pmatrix}\Big|_v = \begin{pmatrix} r_{xx} & r_{xy} \\ r_{yx} & r_{yy} \end{pmatrix}\begin{pmatrix} -E^i\cos(45°) \\ E^i\cos(45°) \end{pmatrix} \\ &= \begin{pmatrix} r_{yy} & r_{xy} \\ r_{xy} & r_{yy} \end{pmatrix}\begin{pmatrix} -E^i\cos(45°) \\ E^i\cos(45°) \end{pmatrix}. \end{aligned} \tag{6}$$

Formula (6) demonstrates that $E^r_x|_u = E^r_y|_u$ or $E^r_x|_v = -E^r_y|_v$, and the polarization direction of the reflected wave is the same as that of the incident wave, and no cross-polarized components exist at the u- and v-polarized incidences. From this passage, we can deduce that the magnitudes of the coreflected coefficients r_{uu} and r_{vv} at u- and v-polarized incidences would both be close to 1.0 because the dielectric loss tangent of the dielectric substrate is very small.

In succession, supposing that the incidence is a y-polarized wave again, the incident field and the reflected field can be expressed as (7) and (8), respectively,

$$E^i = E^i_y\hat{e}_y = E^i_u\hat{e}_u + E^i_v\hat{e}_v = E^i_y\cos(45°)(\hat{e}_u + \hat{e}_v), \tag{7}$$

$$\begin{aligned} E^r &= E^r_u\hat{e}_u + E^r_v\hat{e}_v = r_{uu}E^i_u\hat{e}_u + r_{vv}E^i_v\hat{e}_v \\ &= E^i_y\cos(45°)(r_{uu}\hat{e}_u + r_{vv}\hat{e}_v). \end{aligned} \tag{8}$$

Because of the anisotropy of the unit cell structure, r_{uu} and r_{vv} are mutually independent. In order to facilitate the derivation of formula, we define the actual phase difference between r_{uu} and r_{vv} as $\Delta\varphi$; in addition, because the magnitude of r_{uu} and r_{vv} will both be close to 1.0, we

neglect the dielectric loss and assume their magnitude is just equal to 1.0 in the following derivation process. In this way, $r_{vv} = r_{uu}e^{-j\Delta\varphi}$, and the reflected field can be expressed as

$$E^r = r_{uu}E_y^i\cos(45°)(\hat{e}_u + e^{-j\Delta\varphi}\hat{e}_v). \tag{9}$$

Formula (9) implies that the moving track of the tip of the electric field vector $\boldsymbol{E}^r$ in any fixed plane parallel with the u-v one, which is normal to the direction $-\hat{e}_z$ of propagation, will satisfy the equation

$$E_u^2 - 2E_uE_v\cos\Delta\varphi + E_v^2 = 0.5|E_y^i|^2\sin^2\Delta\varphi. \tag{10}$$

In the x-y coordinate system, using the relationship equations $E_y=(E_u+E_v)\cos(45°)$, $E_x=(E_u-E_v)\sin(45°)$, Eq. (10) can be expressed as

$$\frac{E_x^2}{|E_y^i|^2(1-\cos\Delta\varphi)/2} + \frac{E_y^2}{|E_y^i|^2(1+\cos\Delta\varphi)/2} = 1. \tag{11}$$

Equation (11) implies that the magnitudes of the x- and y-polarized components in the reflected field are

$$|E_x^r| = |E_x|_{E_y=0} = |E_y^i|\sqrt{(1-\cos\Delta\varphi)/2}, \tag{12a}$$

$$E_y^r = |E_y|_{E_x=0} = |E_y^i|\sqrt{(1+\cos\Delta\varphi)/2}, \tag{12b}$$

respectively. In this way, the magnitudes of r_{xy} and r_{yy} can be calculated as follows:

$$|r_{xy}| = \frac{|E_x^r|}{|E_y^i|} = \frac{|E_x|_{E_y=0}}{|E_y^i|} = \sqrt{(1-\cos\Delta\varphi)/2}, \tag{13a}$$

$$|r_{yy}| = \frac{|E_y^r|}{|E_y^i|} = \frac{|E_y|_{E_x=0}}{|E_y^i|} = \sqrt{(1+\cos\Delta\varphi)/2}. \tag{13b}$$

For $\Delta\varphi$ possibly being an arbitrary value depending on the frequency, the above Eqs. (10), (11), and (13) imply that all polarization states including LP, CP, and the elliptical polarization would possibly be realized in the reflected wave at the y-polarized incidence. Commonly, the reflected wave would be elliptically polarized, and the axial ratio can be expressed as $\mathrm{AR} = \sqrt{(1-\cos\Delta\varphi)/(1+\cos\Delta\varphi)}$ according to Eq. (11). When $\Delta\varphi = \pm 90°$, the axial ratio is $\mathrm{AR} = 1.0$, the reflected wave would be converted into a CP one. When $\Delta\varphi = \pm 180°$, Eq. (10) can be simplified as $E_u = -E_v$. In this way, $E^r = E_u\hat{e}_u - E_v\hat{e}_v = \sqrt{2}E_u\hat{e}_x$, and the anticipated LP conversion can be realized in the reflected wave as shown in Fig. 4. In addition, Eq. (13) indicates that $|r_{yy}| = 0$ and $|r_{xy}| = 1$, and a perfect LP conversion can be realized if no dielectric loss exists.

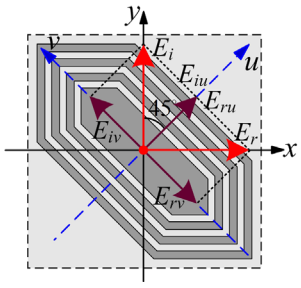

FIG. 4. Intuitive picture of y-to-x polarization conversion in the proposed reflector.

Following the above analysis, to make clear the root cause of the polarization conversion for the reflector, we carry out numerical simulations at u- and v-polarized incidences, respectively. The simulated results in Fig. 5(a) indicate that the magnitudes of r_{uu} and r_{vv} are both much closer to 1.0 in the majority of the frequency range. However, there are still some minimal values existing at the eleven frequencies: 4.27, 5.17, 6.74, 6.98, 8.19, 8.66, 10.68, 12.77, 15.82, and 16.82 GHz, and it is implied that five resonant eigenmodes are excited at the u-polarized incidence and six resonant eigenmodes are excited at the v-polarized incidence. Compared to the datum in Fig. 2(d), these resonant frequencies are almost the same (4.35, 5.17, 6.74, 7.00, 8.20, 8.73, 10.68, 15.58, 15.82, and 16.83 GHz). Only one resonant frequency 12.77 GHz was not found in Fig. 2(d). In fact, for the unit cell structure of the reflector is composed of multiple independent metallic patches printed on a grounded dielectric substrate. It can be equivalent to a combiner of multiple LC parallel resonators, wherein the equivalent capacitance C comes from the charge accumulations between the gap of adjoining metallic patches, which is not a pure capacitance due to the dielectric loss of the grounded dielectric substrate, and the equivalent inductance L results from the surface currents distributed on the metallic patch and grounded plane. Moreover, the unit cell is an anisotropic structure. The values of the equivalent capacitance C and inductance L in each resonator will both be different at u- and v-polarized incidences due to the different directions of incident electric fields, so different eigenmodes will be excited at u- and v-polarized incidences. Figure 5(a) shows that five of these eigenmodes are excited by u-polarized incidences and the other six eigenmodes are excited by v-polarized incidences. Because a y-polarized wave consists of both u- and v-polarized components, the eleven eigenmodes have all been excited by a y-polarized incidence as shown in Fig. 2(d).

Moreover, to know the effect of these eigenmodes on the generation of the multiband polarization conversion, after several simulations, we present in Fig. 6 the surface currents on the two-corner-cut square multiring disk at each eigenfrequency. Figure 6(a) indicates that the first pair of eigenmodes is generated at the outer ring. The surface currents in the first eigenmode are mainly distributed on the

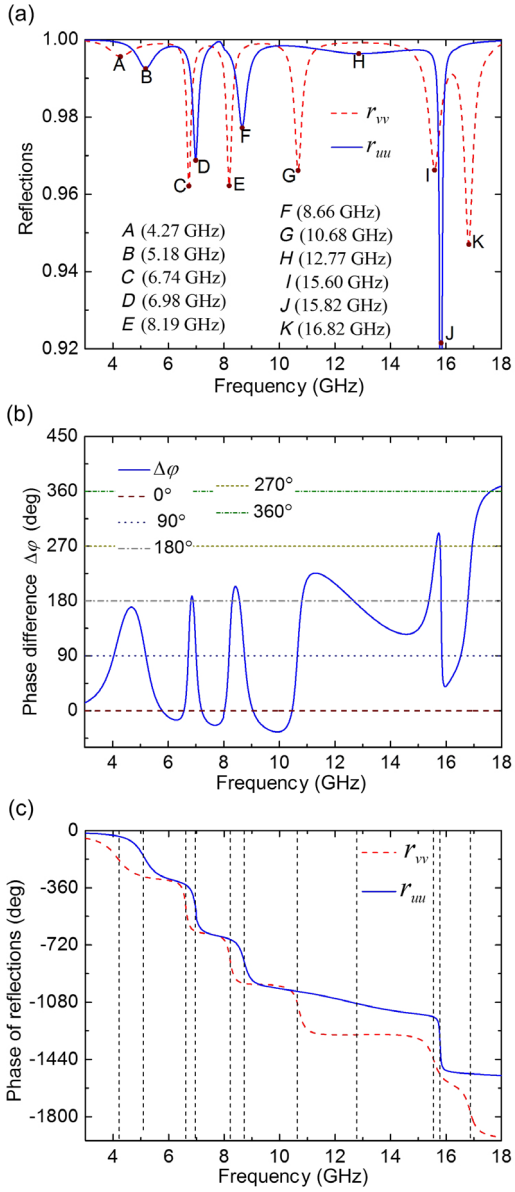

FIG. 5. Simulated results of the reflector at u- and v-polarized incidences: (a) the magnitudes of r_{uu} and r_{vv}, (b) the phase difference $\Delta\varphi$ between r_{uu} and r_{vv}, and (c) the phase variations of r_{uu} and r_{vv} caused by the eigenmodes.

pair of long oblique sides, and the distribution pattern is symmetrical with respect to the v-axis. While those of the second eigenmode are mainly on the two pairs of vertical and level sides, which are symmetrical with respect to the u axis. From this, we can conclude that the first and second eigenmodes are excited by v- and u-polarized incidences, respectively, and the surface currents in the first and second eigenmodes cannot produce u- and v-polarized radiations, respectively, such that no cross-polarized reflection exists at v- and u-polarized incidences when the two eigenmodes are excited. In addition, in Figs. 6(b) and 6(c), it is shown that the next two pairs of eigenmodes are almost the same as the first pair, except that only the two pairs of eigenmodes are generated at the middle and inner rings, respectively. Figure 6(d) indicates that the fourth pair of eigenmodes is generated at the central disk, and Figs. 6(e) and 6(f) indicate that the fifth pair of eigenmodes, together with the last one, are higher-order eigenmodes generated at the outer ring. Because of the symmetrical distributions of the surface currents in these eigenmodes, these surface currents can all be equivalent to a small resonant current in the direction of the v or u axis, which is the same with the polarization direction of the incident wave, so only the copolarized reflection can be produced at v- or u-polarized incidences when any eigenmode is excited. However, when these eigenmodes are excited by y-polarization incidences, cross-polarized reflection will be produced for the x component of the surface currents exists in each eigenmode.

How do we consider the specific effect of these eigenmodes on the polarization conversion at the y-polarization incidence? We can analyze the effect of these eigenmodes on the phases of r_{uu} and r_{vv} because the phase difference $\Delta\varphi$ between r_{uu} and r_{vv} can basically determine the magnitudes of r_{xy} and r_{yy}. Figure 5(b) shows that the data curve of $\Delta\varphi$ fluctuates up and down along with the variable of frequency. It is just equal to 180° at the nine frequencies: 6.82, 6.89, 8.30, 8.57, 10.80, 12.68, 15.38, 15.82, and 16.78 GHz, which implies that the anticipated polarization conversion will be realized at these frequencies. To explain the detailed reasons, the phase variations of r_{uu} and r_{vv} caused by these eigenmodes are shown in Fig. 5(c), in which the affect of the wave path has been eliminated. It is indicated that the phases of r_{vv} and r_{uu} are decreased rapidly at their respective eigenfrequencies for the eigenmodes and can be equivalent to a parallel LC resonance. However, at a certain frequency range centered at the eigenfrequency 12.77 GHz, the phase of r_{uu} is decreased very slowly, it is because the surface currents in this eigenmode are transversely distributed on the narrow and long central disk, as shown in Fig. 6(d), the equivalent inductance L of the surface currents is very little, and the quality factor of this eigenmode is very small. After the analysis of Fig. 5(c), we can clearly understand the root cause of the multiband polarization conversion. The first four bands result from the first four pairs of the first-order eigenmodes, which are generated at the four independent metallic patches: the outer, middle, and inner rings, and the central disk, successively. Now if the reflector is equivalent to a combiner of four resonators, they come from the four resonators, respectively. The two eigenmodes in each pair are successively excited by v- and u-polarized incidences due to the anisotropy of the unit cell structure. A larger phase difference $\Delta\varphi$ between r_{uu} and r_{vv} can be obtained at the frequency range between the two eigenfrequencies. When the anisotropy of the unit cell structure is appropriate, the anticipated polarization conversion can be realized in this frequency range. The first three bands

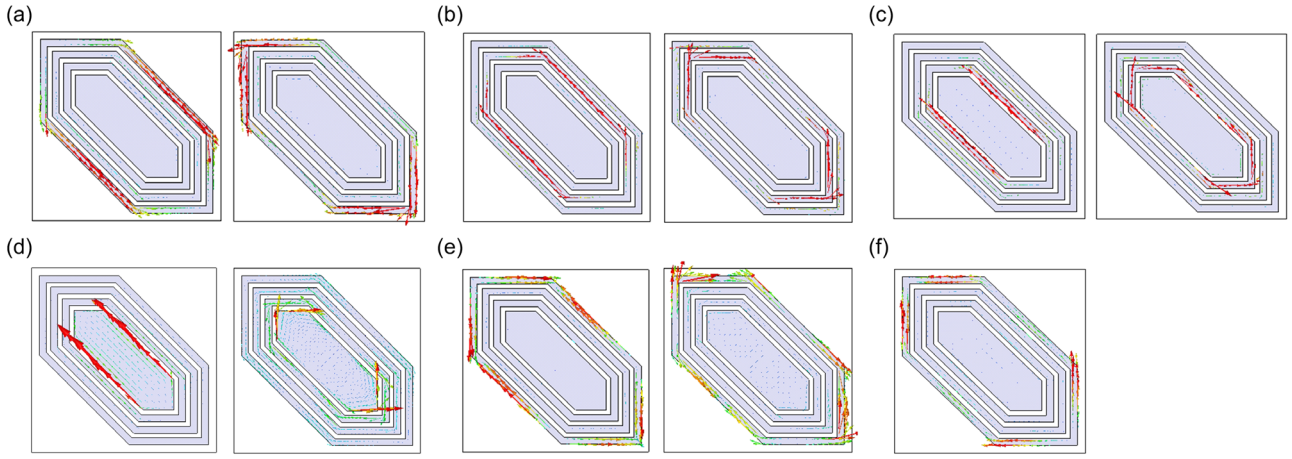

FIG. 6. The surface current distributions at each eigenfrequency: (a) the first pair of eigenmodes (4.27 and 5.18 GHz), (b) the second pair (6.74 and 6.98 GHz), (c) the third pair (8.19 and 8.66 GHz), (d) the fourth pair (10.68 and 12.77 GHz), (e) the fifth pair (15.60 and 15.82 GHz), and (f) the last one (16.82 GHz).

are all just achieved in this way, they all have a certain bandwidth. However, the fourth band is an ultrawideband, which has not been ended by the second eigenmode in the fourth pair due to the small quality factor of this eigenmode. Conversely, it has been widened for the small phase variation of r_{uu}. From this we can learn how to achieve an ultrawideband polarization conversion, because each eigenmode from emergence to termination will change the phases of r_{vv} or r_{uu} by almost 360°. Only when multiple eigenmodes are alternately excited at different frequencies at v- and u-polarized incidences and the quality factors of these eigenmodes are not too large, the phase difference $\Delta\varphi$ can be close to 180° over a wide frequency range, thus achieving ultrawideband polarization conversion. We have analyzed several ultrawideband polarization converters proposed in Refs. [7–11] in detail. In fact, they are all achieved in this way. In our design, the fourth band is started by the first eigenmode in the fourth pair, widened by the second one of the fourth pair, and finally terminated by the first one of the fifth pair, which only results from three eigenmodes, so its relative bandwidth is still not very wide—only 36.8%. In addition, the last two eigenmodes both give rise to a polarization conversion band independently. This is because when the phase of r_{vv} or r_{uu} is changed at a narrow frequency range centered at their eigenfrequencies, the phase of the other one has remained unchanged, such that the two bands are both very narrow. This is particularly the case for the one produced by the second eigenmode of the fifth pair, which has been neglected in the front.

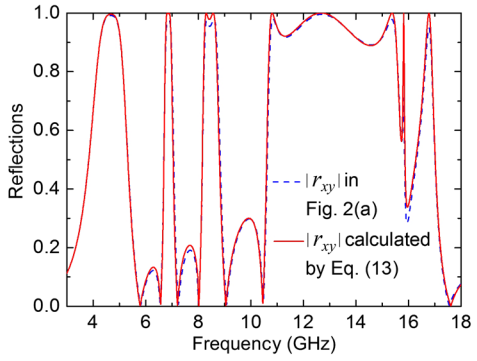

FIG. 7. The comparison between the simulated and calculated results of the cross-polarized reflection coefficients r_{xy}.

Finally, to validate Eq. (13), we calculate the magnitudes of r_{xy} and r_{yy} using Eq. (13) according to the phase differences $\Delta\varphi$ in Fig. 5(b). The calculated results are shown in Fig. 7. It is shown that the calculated results are essentially in agreement with the simulated results at the y-polarized incidence in Fig. 2(a). There is a small difference between them. It is just because the derivation of formula (13) is based on the assumption that no dielectric loss exists. From the above analysis, we can conclude that the anisotropy of the unit cell structure is the root cause of the polarization conversion, which results in multiple different eigenmodes being excited at v- and u-polarized incidences, such phase differences $\Delta\varphi$ between r_{uu} and r_{vv} are generated. The phase differences $\Delta\varphi$ can basically determine the polarization states of the reflected wave. When $\Delta\varphi$ is close to 180°, the anticipated 90° polarization rotation will be realized at x- and y-polarized incidence.

IV. EXPERIMENTAL RESULTS

To verify our design, an experimental sample is fabricated by the conventional printed circuit board process, which contains 25×25 unit cells, covering an area of about 300 mm × 300 mm, as shown in Fig. 8(a). First, to validate its LP-conversion performance, we have measured its co- and cross-polarized reflection coefficients at the y-polarized incidence in a microwave anechoic chamber. The schematic illustration of our measurement setup is shown in Fig. 8(b),

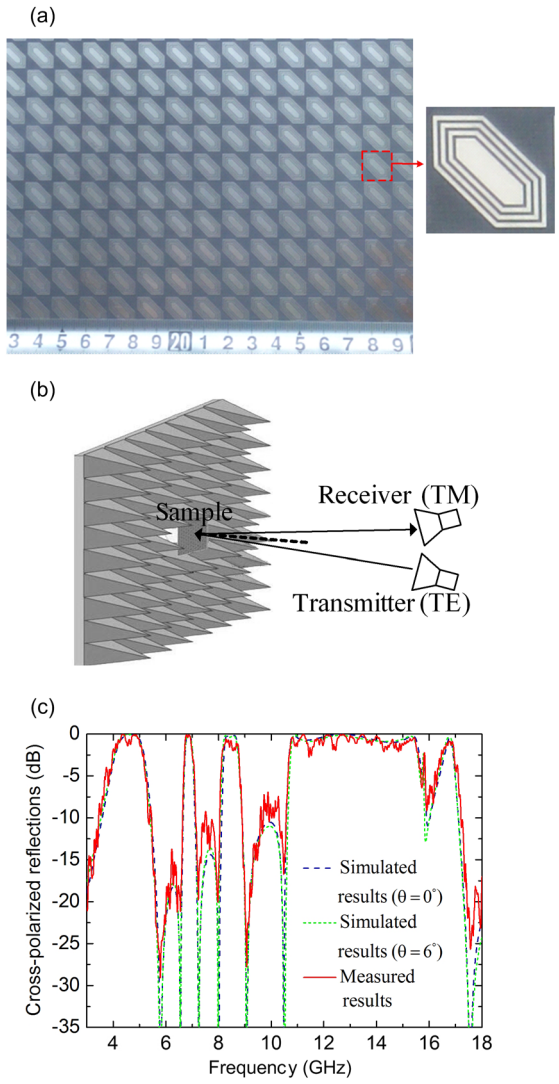

FIG. 8. The fabricated sample and measured results: (a) the photograph of the experimental sample, (b) the schematic of the measurement setup, and (c) the comparison between the simulated and measured results of the cross-polarized reflection coefficient r_{xy}.

in which two identical LP standard-gain horn antennas as transmitter and receiver are connected to the two ports of an Agilent E8363B Agilent network analyzer. In addition, the two horn antennas are set symmetrically with respect to the normal with a small angle of 6° due to the finite sizes of the fabricated sample. The co- and cross-polarized reflection coefficients are measured when the receiving horn antenna rotates by 0° and 90°, respectively. The measured results, together with the simulated results at the vertical incidence and an oblique incidence with 6° incident angle, are shown in Fig. 8(c). It is indicated that the two simulation results are almost the same, for the incident angle of the oblique incidence is very small. In addition, the experimental results are basically in agreement with the simulations. But in several frequency ranges (7.32–7.85 GHz, 9.57–10.37 GHz, 15.86–16.12 GHz, and 17.55–18.00 GHz), wherein the cross-polarized reflection coefficients are small, the experimental results are slightly larger than the simulated ones. The main reason for this phenomenon is that the size of the experimental sample is very limited. A relatively large cross-polarized scattered wave will maybe be generated due to the edge scattering effect of the experimental sample. Moreover, it will look larger when the cross-polarized reflected wave is smaller. In addition, compared with the infinite plate in the simulation, the reflection of each unit cell in the experimental sample structure will also be a little different. Second, to validate its CP-maintaining performance at CP incidence, CP emitters and CP receivers are required. Though the CP antennas exist, they only can produce a high pure CP radiated wave in a narrow frequency range and are not suitable for broadband measurements. Recently, the measurements of the reflections at CP incidence were almost all done by the method of measuring the reflection matrix $\mathbf{R}_{\text{lin}}$ at LP incidence [16,17,40]. When the reflection matrix $\mathbf{R}_{\text{lin}}$ has been measured, the reflection matrix $\mathbf{R}_{\text{cir}}$ at the CP incidence can be obtained by using formula (2). For the proposed reflector, formula (2) can be simplified as formula (5), wherein $|r_{++}| = |r_{--}| = |r_{xy}| = |r_{yx}|$, so the measured results in Fig. 8(c) can also be regarded as the magnitudes of the copolarized reflected coefficients at RHCP and LHCP incidences, which can be used to validate the CP-maintaining performance of the reflector.

V. CONCLUSIONS

In this paper, a multiple-band LP conversion and CP-maintaining reflector using an anisotropic metasurface is proposed, which is composed of a square array of a two-corner-cut square multiring disk printed on grounded dielectric substrate. Both the simulated and experimental results show that the reflector can convert a y-polarized incident wave to its cross-polarized wave in five frequency bands. The first four bands all have a certain bandwidth, the PCR is over 90% in the former three bands, and the fourth band is an ultrawideband. In addition, because of the symmetry of the reflector structure, its cross- and copolarized reflected coefficients at y-polarized incidence are just equal to those at x-polarized incidence. Thus the reflector can realize a CP-maintaining reflection at the same time, moreover, $|r_{++}| = |r_{--}| = |r_{xy}| = |r_{yx}|$. Furthermore, we analyze the root cause of the multiband polarization conversion, and conclude that it is just the anisotropy of the unit cell structure which results in multiple different eigenmodes excited at v- and u-polarized incidences; such a phase difference $\Delta\varphi$ between r_{uu} and r_{vv} will be produced. When $\Delta\varphi$ is close to 180°, the anticipated 90° polarization rotation can be realized at x- and y-polarized incidence. In addition, if multiple eigenmodes can be alternately excited at different frequencies at v- and u-polarized incidences, and the quality factors of these eigenmodes are not too large, such $\Delta\varphi$ can be close to 180°

over a wide frequency range, and an ultrawideband polarization conversion will be achieved. Finally, one experiment is carried out, and the simulated and measured results are in good agreement with each other. Compared with the previous designs, the proposed reflector, as an alternative multiband polarization converter, has more frequency bands, wider bandwidth, and more functions, so it is of a great application value in polarization controlled devices, stealth surfaces, antennas, etc.

ACKNOWLEDGMENTS

This work is supported by the National Nature Science Foundation of China (61471387), the research center for the internet of things and big data technology of Xijing University.

[1] Y. B. Chen, T. B. Chen, Y. C. Jiao, and F. S. Zhang, A reconfigurable microstrip antenna with switchable polarization, J. Microwaves **20**, 1391 (2008).
[2] F. Aldhubaib and N. V. Shuley, Radar target recognition based on modified characteristic polarization states, IEEE Trans. Aerosp. Electron. Syst. **46**, 1921 (2010).
[3] Y. Jia, Y. Liu, Y. J. Guo, K. Li, and S. X. Gong, Broadband polarization rotation reflective surfaces and their applications to RCS reduction, IEEE Trans. Antennas Propag. **64**, 179 (2016).
[4] Y. Liu, K. Li, Y. Jia, Y. Hao, S. Gong, and Y. J. Guo, Wideband RCS reduction of a slot array antenna using polarization conversion metasurfaces, IEEE Trans. Antennas Propag. **64**, 326 (2016).
[5] L. Young, L. A. Robinson, and C. A. Hacking, Meander-line polarizer, IEEE Trans. Antennas Propag. **21**, 376 (1973).
[6] Y. H. Huang, Y. Zhou, and S. T. Wu, Broadband circular polarizer using stacked chiral polymer films, Opt. Express **15**, 6414 (2007).
[7] H. Chen, J. Wang, H. Ma, and S. Qu, Ultra-wideband polarization conversion metasurfaces based on multiple plasmon resonances, J. Appl. Phys. **115**, 177403 (2014).
[8] X. Gao, X. Han, W. Cao, H. O. Li, H. F. Ma, and T. J. Cui, Ultrawideband and high-efficiency linear polarization converter based on double V-shaped metasurface, IEEE Trans. Antennas Propag. **63**, 3522 (2015).
[9] S. Sui, H. Ma, J. Wang, M. Feng, Y. Pang, S. Xia, Z. Xu, and S. Qu, Symmetry-based coding method and synthesis topology optimization design of ultra-wideband polarization conversion metasurfaces, Appl. Phys. Lett. **109**, 014104 (2016).
[10] G. Dong, H. Shi, S. Xia, W. Li, A. Zhang, X. Zhuo, and X. Wei, Ultra-broadband and high-efficiency polarization conversion metasurface with multiple plasmon resonance modes, Chin. Phys. B **25**, 084202 (2016).
[11] M. I. Khan, Q. Fraz, and F. A. Tahir, Ultra-wideband cross polarization conversion metasurface insensitive to incidence angle, J. Appl. Phys. **121**, 045103 (2017).
[12] P. Su, Y. Zhao, S. Jia, W. Shi, and H. Wang, An ultrawideband and polarization-independent metasurface for RCS reduction, Sci. Rep. **6**, 20387 (2016).
[13] H. Sun, C. Gu, X. Chen, Z. Li, L. Li, and F. Martion, Ultrawideband and broad-angle linear polarization conversion metasurface, J. Appl. Phys. **121**, 1304 (2017).
[14] P. Xu, S. Y. Wang, and W. Geyi, A linear polarization converter with near unity efficiency in microwave regime, J. Appl. Phys. **121**, 1804 (2017).
[15] M. Mutlu and E. Ozbay, A transparent 90° polarization rotator by combining chirality and electromagnetic wave tunneling, Appl. Phys. Lett. **100**, 051909 (2012).
[16] L. Wu, Z. Yang, Y. Cheng, R. Gong, M. Zhao, Y. Zheng, J. Duan, and X. Yuna, Circular polarization converters based on bi-layered asymmetrical split ring metamaterials, Appl. Phys. A **116**, 643 (2014).
[17] J. Kaschke, L. Blume, L. Wu, M. Thiel, K. Bade, Z. Yang, and M. Wegener, A helical metamaterial for broadband circular polarization conversion, Adv. Opt. Mater. **3**, 1411 (2015).
[18] X. Ma, Z. Xiao, and D. Liu, Dual-band cross polarization converter in bi-layered complementary chiral metamaterial, J. Mod. Opt. **63**, 937 (2016).
[19] G. Zhou, X. Tao, Z. Shen, G. Zhu, B. Jin, L. Kang, W. Xu, J. Chen, and P. Wu, Designing perfect linear polarization converters using perfect electric and magnetic conducting surfaces, Sci. Rep. **6**, 38925 (2016).
[20] V. V. Klimov, I. V. Zabkov, A. A. Pavlov, R. C. Shiu, H. C. Chan, and G. Y. Guo, Manipulation of polarization and spatial properties of light beams with chiral metafilms, Opt. Express **24**, 6172 (2016).
[21] W. Xu, Y. Shi, J. Ye, F. Ren, I. V. Shadrivov, and H. Lu, A terahertz controlled-NOT gate based on asymmetric rotation of polarization in chiral metamaterials, Adv. Opt. Mater. **5**, 1700108 (2017).
[22] Y. Liu, Y. Luo, C. Liu, K. Song, and X. Zhao, Linear polarization to left/right-handed circular polarization conversion using ultrathin planar chiral metamaterials, Appl. Phys. A **123**, 571 (2017).
[23] J. K. Gansel, M. Thiel, M. S. Rill, M. Decker, K. Bade, V. Saile, G. V. Freymann, S. Linden, and M. Wegener, Gold helix photonic metamaterial as broadband circular polarizer, Science **325**, 1513 (2009).
[24] J. Kaschke, L. Blume, L. Wu, M. thiel, K. Bade, Z. Yang, and M. Wegener, A helical metamaterial for broadband circular polarization conversion, Adv. Opt. Mater. **3**, 1411 (2015).
[25] R. Ji, S. Wang, X. Liu, X. Chen, and W. Lu, Broadband circular polarizers constructed using helix-like chiral metamaterials, Nanoscale **8**, 14725 (2016).
[26] M. L. N. Chen, L. J. Jiang, W. E. I. Sha, W. C. H. Choy, and T. Itoh, Polarization control by using anisotropic 3-D chiral structures, IEEE Trans. Antennas Propag. **64**, 4687 (2016).
[27] C. Pfeiffer, C. Zhang, V. Ray, J. Guo, and A. Grbic, High Performance Bianisotropic Metasurfaces: Asymmetric Transmission of Light, Phys. Rev. Lett. **113**, 023902 (2014).
[28] Y. Xu, Q. Shi, Z. Zhu, and J. Shi, Mutual conversion and asymmetric transmission of linearly polarized light in bilayered chiral metamaterial, Opt. Express **22**, 25679 (2014).

[29] D. Liu, Z. Xiao, X. Ma, L. Wang, K. Xu, J Tang, and Z. Wang, Dual-band asymmetric transmission of chiral metamaterial based on complementary U-shaped structure, Appl. Phys. A **118**, 787 (2015).
[30] S. Fang, K. Luan, H. F. Ma, W. Lv, Y. Li, Z. Zhu, C. Guan, J. Shi, and T. J. Cui, Asymmetric transmission of linearly polarized waves in terahertz chiral metamaterials, J. Appl. Phys. **121**, 033103 (2017).
[31] X. Huang, D. Yang, and H. Yang, Multiple-band reflective polarization converter using U-shaped metamaterial, J. Appl. Phys. **115**, 103505 (2014).
[32] X. Huang, B. Xiao, L. Guo, S. Yu, and H. Yang, Triple-band linear and circular reflective polarizer based on E-shaped metamaterial, J. Opt. **16**, 125101 (2014).
[33] J. Ding, B. Arigong, H. Ren, M. Zhou, J. Shao, Y. Lin, and H. Zhang, Efficient multiband and broadband cross polarization converters based on slotted L-shaped nanoantennas, Opt. Express **22**, 29143 (2014).
[34] J. Zhao, B. Xiao, X. Huang, and B. Xiao, Multiple-band reflective polarization converter based on complementary L-shaped metamaterial, Microwave Opt. Technol. Lett. **57**, 978 (2015).
[35] H. Li, B. Xiao, X. Huang, and H. Yang, Multiple-band reflective polarization converter based on deformed F-shaped metamaterial, Phys. Scr. **90**, 035806 (2015).
[36] K. Song, Y. Liu, C. Luo, and X. Zhao, High-efficiency broadband and multiband cross-polarization conversion using chiral metamaterial, J. Phys. D **47**, 505104 (2014).
[37] A. E. Serebryannikov, M. Mutlu, and E. Ozbay, Dielectric inspired scaling of polarization conversion subwavelength resonances in open ultrathin chiral structures, Appl. Phys. Lett. **107**, 221907 (2015).
[38] D. J. Liu, Z. Y. Xiao, and Z. H. Wang, Multi-band asymmetric transmission and 90° polarization rotator based on bilayered metasurface with *F*-shaped structure, Plasmonics **12**, 445 (2017).
[39] X. Huang, J. Chen, and H. Yang, High-efficiency wideband reflection polarization conversion metasurface for circularly polarized waves, J. Appl. Phys. **122**, 076401 (2017).
[40] Y. Li, J. Zhang, S. Qu, J. Wang, L. Zheng, H. Zhou, Z. Xu, and A. Zhang, Wide-band circular polarization-keeping reflection mediated by metasurface, Chin. Phys. B **24**, 014202 (2015).
[41] Y. Li, J. Zhang, S. Qu, J. Wang, X. Wu, Z. Xu, and A. Zhang, Circularly polarized wave reflection focusing metasurfaces, Acta Phys. Sin. **64**, 124102 (2015).
[42] Y. Li, J. Zhang, S. Qu, J. Wang, X. Wu, Z. Xu, and A. Zhang, Design and verification of a two-dimensional wide band phase-gradient metasurface, Acta Phys. Sin. **64**, 094101 (2015).
[43] J. Yang, S. Qu, H. Ma, J. Wang, S. Sui, and Q. Zheng, Ultrabroadband co-polarization anomalous reflection metasurface, Appl. Phys. A **123**, 537 (2017).